

Salicylanilides Reduce SARS-CoV-2 Replication and Suppress Induction of Inflammatory Cytokines in a Rodent Model

Steven Blake,¹ Namir Shaabani,¹ Lisa M. Eubanks, Junki Maruyama, John T. Manning, Nathan Beutler, Slobodan Paessler, Henry Ji, John R. Teijaro, and Kim D. Janda*



Cite This: *ACS Infect. Dis.* 2021, 7, 2229–2237



Read Online

ACCESS |



Metrics & More



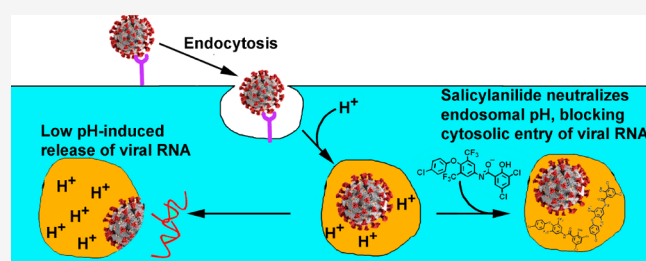
Article Recommendations



Supporting Information

ABSTRACT: SARS-CoV-2 virus has recently given rise to the current COVID-19 pandemic where infected individuals can range from being asymptomatic, yet highly contagious, to dying from acute respiratory distress syndrome. Although the world has mobilized to create antiviral vaccines and therapeutics to combat the scourge, their long-term efficacy remains in question especially with the emergence of new variants. In this work, we exploit a class of compounds that has previously shown success against various viruses. A salicylanilide library was first screened in a SARS-CoV-2 activity assay in Vero cells. The most efficacious derivative was further evaluated in a prophylactic mouse model of SARS-CoV-2 infection unveiling a salicylanilide that can reduce viral loads, modulate key cytokines, and mitigate severe weight loss involved in COVID-19 infections. The combination of anti-SARS-CoV-2 activity, cytokine inhibitory activity, and a previously established favorable pharmacokinetic profile for the lead salicylanilide renders salicylanilides in general as promising therapeutics for COVID-19.

KEYWORDS: SARS-CoV-2, salicylanilides, cytokines, antiviral, ionophore



After claiming its first victims in Wuhan, China, via zoonotic transmission at the end of 2019, the novel severe acute respiratory syndrome coronavirus 2 (SARS-CoV-2), the causative agent of COVID-19, metastasized into a global plague, which triggered a staggering death toll in the millions and ground national economies worldwide to a halt over a period of just a few months. On March 11, 2020, the World Health Organization (WHO) officially declared COVID-19 a global pandemic as population centers in over 100 countries had become exposed to the virus. In the US alone as of July 2021, COVID-19 killed more than 610 000 people and is projected to cost Americans an estimated \$16 trillion over the next 10 years due to devastating loss of gross domestic product and overwhelming healthcare expenses.¹

The economic and humanitarian turmoil caused by COVID-19 has been facilitated by the virus's insidious capacity to efficiently spread from person to person. In many cases, mildly symptomatic or asymptomatic individuals who compose most of the infected people unknowingly expose the elderly and already infirmed segments of the population to the virus through aerosolized respiratory particles. After inhalation of these small virus-containing droplets, the viral particles can enter host cells through binding of the viral surface spike proteins to the host ACE-2 receptors, which are highly expressed on the epithelial cells in the nasal and upper respiratory tract. After clathrin-mediated endocytosis into the host cell, viral-endosomal membrane fusion that is triggered by

the acidic endosomal environment releases the viral RNA into the cytosol.^{2–4} Without endosomal escape, the virus is either shuttled back to the extracellular space or degraded in the harsh environment of the lysosome.⁵ Once inside the cytosol, SARS-CoV-2 hijacks the host machinery producing new viral particles that upon secretion can infect more cells in the lower respiratory tract and further propagate or be released via respiratory droplets and transmitted to other individuals.

Infected individuals who are at least 40 years of age have a higher likelihood of developing severe symptoms that can ultimately result in acute respiratory distress syndrome (ARDS). The path to this life-threatening condition starts when infected alveolar epithelial cells release inflammatory markers and cytokines into the air space of the lungs that subsequently draw T-cells to the inflammation site. The combination of T-cell accumulation in this area and viral replication-induced apoptosis of pneumocytes causes significant injury to the lung tissue, thereby making the exchange of oxygen and carbon dioxide across the alveolar epithelium increasingly difficult and possibly fatal.²

Received: May 6, 2021

Published: August 2, 2021



Despite the devastation that COVID-19 has wreaked, preventative medicine has attained some success in curtailing new cases. Currently, there are three vaccine formulations in the US by Moderna, Pfizer-BioNTech, and Johnson & Johnson that have received emergency use authorization (EUA) by the Food and Drug Administration (FDA). While approximately half of the population has begun the immunization process as of now, achieving “herd immunity”, where 70% of the population is protected either by vaccination or from prior infection, is not realistically expected in the near future due to vaccine apprehension and concerns over potential side effects in combination with the continuous emergence of new SARS-CoV-2 variants⁶ such as B.1.617.2 (Delta).

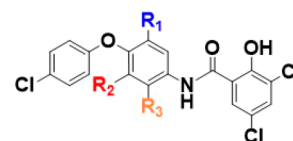
With close to 35 million in the US and 200 million worldwide already infected with SARS-CoV-2 and the uncertainty of herd immunity in the near term, the value of antivirals and neutralizing antibodies against SARS-CoV-2 becomes significant. Currently, the FDA has approved remdesivir and granted EUA for several monoclonal antibodies (mAbs) such as bamlanivimab and etesevimab as they have shown efficacy in reducing the severity of symptoms and viral load.^{7–9} However, remdesivir was authorized for hospitalized individuals; the leading arsenal of mAbs has yet to complete Phase 3 clinical trials and has recently shown reduced efficacy toward new SARS-CoV-2 variants.^{10,11} Therefore, new antivirals that can blunt the symptoms of infection early on and have broad antiviral activity to combat imminent variants remain in dire need.

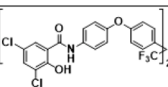
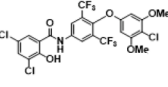
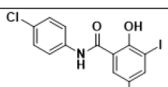
One potential COVID-19 therapeutic that has shown broad efficacy against viruses including SARS-CoV-2 is niclosamide, an FDA-approved antihelmintic.^{12–18} This salicylanilide’s antiviral activity stems from its ability to prevent acidification of endocytotic compartments, thereby blocking membrane fusion and infection of the host cell. Moreover, early viral studies demonstrated that the efficacy of salicylanilides was reduced when electron-withdrawing groups were added to the anilide ring, thus demonstrating the important role of the N–H group in shuttling protons into the endosome.¹² Niclosamide’s ability to reduce infection of cells without interacting directly with any viral components creates the prospect to develop anti-COVID-19 therapeutics with broad activity against current and future variants of the virus. However, in saying this, niclosamide is not an optimal antiviral drug option as it is gut restricted and has cellular toxicity issues.^{19,20} In light of the considerations discussed above, an evaluation of a salicylanilide library might provide molecules with improved properties over niclosamide. The research described herein details the efficacy of these analogues against the virus *in vitro*, and the most potent molecule emerging from these cell studies was examined for viral load reduction, prevention of weight loss, and inflammatory markers in a prophylactic mouse model of SARS-CoV-2 infection.

The salicylanilide class’s protonophore properties²¹ strongly rely on an acidic phenolic OH on the salicyl-ring and an amide proton for antimicrobial activity²² although niclosamide’s amide proton seems to be a stronger contributor against viruses.¹² Based on our recent work examining salicylanilides for the treatment of *Clostridioides difficile* infections,^{23,24} we explored the inductive effect on their protic substituents by enlisting a series of analogues (1–13) that carry functional groups ranging from strongly electron-donating (methoxy, 7) to electron-withdrawing (dinitro, 13) (Table 1) in hopes of

finding a more effective salicylanilide antiviral against COVID-19.

Table 1. Reduction of Viral Activity by Salicylanilide Analogues with 11 Being the Most Efficacious



Entry	-R ₁	-R ₂	-R ₃	Log reduction of viral infectivity ^a
1	H	H	H	0.2
2	H	H	Br	0.4
3	Br	H	H	0.7
4	Cl	H	H	2.7
5	I	H	H	0.4
6	F	H	H	0.4
7	OMe	H	H	2.2
8	H	H	OMe	0.0
9	CN	H	H	0.4
10	H	H	I	-0.3
11	CF ₃	CF ₃	H	3.4
12	I	I	H	2.0
13	NO ₂	NO ₂	H	1.7
closantel	*	*	*	0
niclosamide	*	*	*	2.2
oxyclozanide	*	*	*	1.7
rafoxanide	*	*	*	0.2
 14	*	*	*	3.0
 15	*	*	*	2.4
 16	*	*	*	2.7
+ control ^b	*	*	*	0.0
- control ^c	*	*	*	5.7

^aCalculated by subtracting the log(TCID₅₀/mL) of each compound from a positive control. Assays were performed in triplicate ^bNo compounds were added to cells. ^cNo compounds and no virus were added to cells.

We began by examining the efficacy of the salicylanilides using a SARS-CoV-2 cell-based assay (Table 1). In brief, Vero cells were pretreated with 20 μM compound for 4 h followed by inoculation with SARS-CoV-2 at a multiplicity of infection (MOI) of 0.05. After 24 h postinfection, the SARS-CoV-2 titers in Vero cells were determined by a 50% tissue culture infectious disease dose assay (TCID₅₀). Results of this assay

demonstrated that salicylanilide **11** displayed the best efficacy in reducing viral infectivity among compounds tested (Table 1). To account for these findings, we reason that the bis(trifluoromethyl) substituents on **11** impart the amide proton with acid/base properties that best prevent acidification of endosomes among the salicylanilides tested.

Subsequently, we further probed the efficacy of the seven most potent salicylanilides (**11**, **16**, **4**, **15**, **7**, **12**, and niclosamide) at varying concentrations. Using the aforementioned cell-based assay approach but with a 72 h postinfection period, **11** and niclosamide showed the best activity against the virus (Figure 1) with comparable IC_{50} s at $0.74 \mu\text{M}$. The others

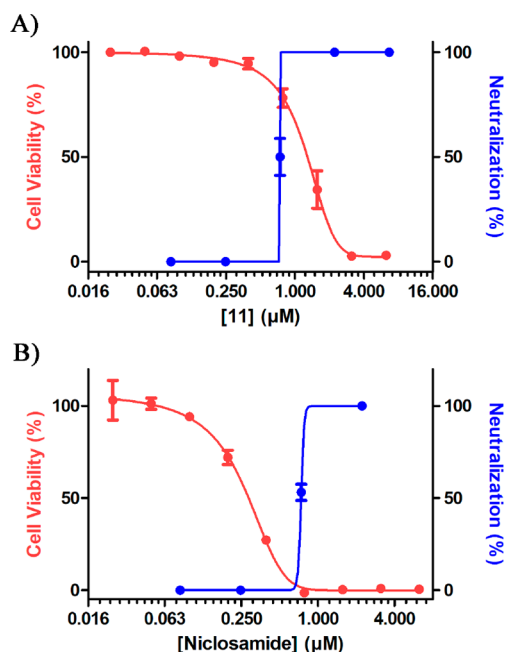


Figure 1. Graphs comparing cell viability and neutralization of viral activity as a function of drug concentration for (A) **11** and (B) niclosamide. Assays were run in duplicate.

displayed either less or negligible activity (Figure S1). Then, the toxicity of **11** and niclosamide with untreated Vero cells was evaluated using an ATP-based cell viability assay with a 72 h exposure period to the drugs. Niclosamide ($EC_{50} = 0.25 \pm 0.011 \mu\text{M}$) showed about a 5-fold greater toxicity than **11** ($EC_{50} = 1.22 \pm 0.031 \mu\text{M}$). Moreover, **11**'s therapeutic index (1.65) is significantly better than niclosamide's (0.34), and we would suggest that much of niclosamide's perceived antiviral activity stems from its cellular toxicity (Figure 1).

Notable is **11**'s superiority at curbing viral replication without a major loss in viability (Table 1 and Figure 1) over niclosamide, which is currently in clinical trials as an oral anti-COVID-19 drug.^{25,26} Salicylanilide **11** also carries less pharmacokinetic liability than niclosamide as it can be administered orally, yet with a 76% systemic bioavailability²³ in mice in contrast to niclosamide's 10%.²⁰ Additionally, systemic toxicity from **11** was negligible at an oral twice-daily dose of 5 mg/kg for 5 days (Figure S2). Moreover, in HEK 293T/17 human kidney cells, **11** presents much less toxicity than niclosamide.²³ Finally, if endosomal acidification is the critical feature for salicylanilides to block SARS-CoV-2 cellular proliferation, then these molecules would be equally effective against recent emerging variants.

After establishing **11** as the best analogue in the *in vitro* cell-based assay, we moved forward with evaluating its performance in a prophylactic mouse model of SARS-CoV-2 infection. A key parameter in this study was the use of molnupiravir (also known as EDD-2801/MK-4482), which is a prodrug of the antiviral ribonucleoside analogue β -D-N4-hydroxycytidine (NHC; EIDD-1931). Our choice for using molnupiravir was based upon its ability to treat infections caused by multiple RNA viruses including SARS-CoV-2.^{27,28} Experimental parameters involved three groups of transgenic hACE-2 mice ($n = 5$) where each group was orally administered either vehicle (negative control), molnupiravir (EIDD-2801, positive control) at 500 mg/kg, or **11** at 5 mg/kg (Day 0). The oral doses were administered twice a day at 12 h intervals for a total of 5 days. 24 h after the first dose, all three groups were intranasally infected with 10 000 plaque-forming units (PFU) of SARS-CoV-2 on Day 1 (Figure 2). The nontreated group (vehicle)

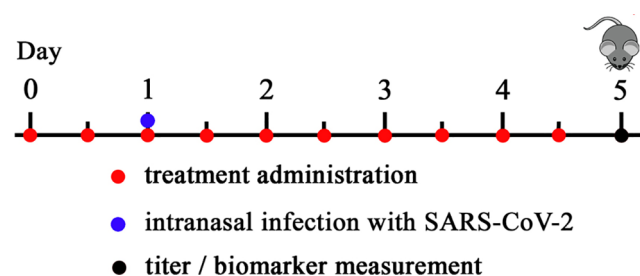


Figure 2. Schedule of the prophylactic mouse model of SARS-CoV-2.

averaged a 10% weight loss by Day 4 while the treated groups (**11** and EIDD-2801) displayed no clinical signs and maintained healthy weights throughout the course of the experiment (Figure 3A).

Lung viral titer results revealed that mice treated with **11** averaged approximately 10-fold lower viral titers than the vehicle with EIDD-2801 displaying no measurable titer levels (Figure 3B). COVID-19 is characterized by an early stage of viral replication followed in some cases by overproduction of inflammatory cytokines, the so-called cytokine storm syndrome (CSS).²⁹ Indeed, CSS has been proposed as underlying the etiology of respiratory failure in patients with COVID-19. We were thus led to ask whether **11** might serve to reduce inflammatory cytokine production. Toward this end, the concentrations of various cytokines in the bronchoalveolar lavage fluids from the three treatment groups of mice were examined (Figure 4). Specifically, the effects of **11** on the interleukin-6 (IL-6), monocyte chemoattractant protein-1 (MCP-1), granulocyte-macrophage colony-stimulating factor (G-CSF), and eotaxin concentrations were examined due to their upregulation in and predictive value for severe cases of COVID-19 in patients.^{30–34} Compound **11** managed to reduce IL-6, MCP-1, and G-CSF levels by 8-, 3.5-, and 10-fold, respectively, relative to untreated mice (Figure 4A–C). Moreover, with respect to IL-6 and MCP-1, the reduction of cytokine concentrations was on par with EIDD-2801 (Figure 4A,C). However, a significant difference in the concentration of eotaxin was not observed in the three groups of mice (Figure 3D).

The findings from the SARS-CoV-2 mouse model illustrate that **11** can partially suppress viral replication in the host, presumably by preventing the acidification of the endocytic compartment. Most gratifying was **11**'s capacity to also prevent

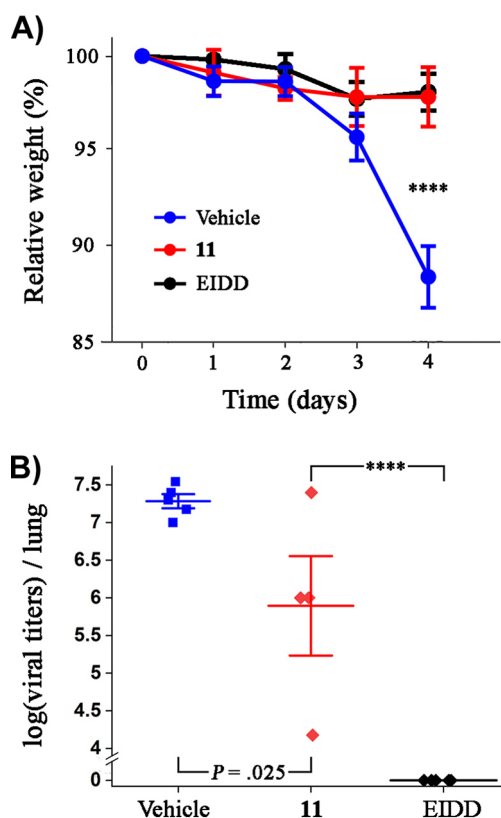


Figure 3. (A) Weight loss in mice monitored throughout the duration of the dosing schedule. (B) Impact of orally administered compounds on the viral titers in the lungs on Day 4. **** $P < 0.0001$.

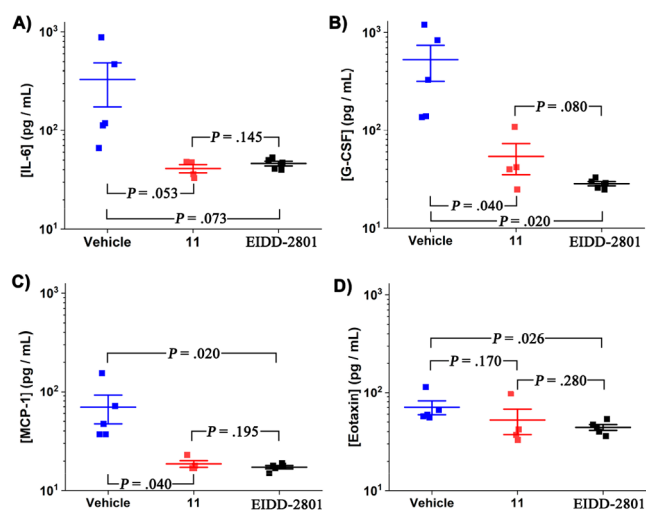


Figure 4. Graphs illustrating the influence of 11 and EIDD-2801 on the cytokine levels of (A) IL-6, (B) G-CSF, (C) MCP-1, and (D) eotaxin in the three treatment groups.

elevation of key contributors of inflammation typically found in the more advanced stages of COVID-19. It was noteworthy that 11 was dosed approximately 100-fold less than EIDD-2801. Taken together, this suggests that salicylanilides could present a dual mechanism of action against SARS-CoV-2, one that both inhibits viral replication and attenuates the production of a subset of inflammatory cytokines.

The COVID-19 pandemic has created an urgent need for therapeutics that inhibit the SARS-CoV-2 virus and suppress

the severe onset of inflammation, a characteristic of advanced illness. The simple screening of a small salicylanilide library has led to the discovery of a compound that can reduce viral titers, weight loss associated with viral infection, as well as lung inflammation in a mouse model. The lead salicylanilide is orally bioavailable, and based upon its proposed mechanism of action should be equally effective against emerging SARS-CoV-2 variants. The unique viral and inflammatory modulation that the salicylanilides present paves the way for further exploration into this class of molecule for the treatment of COVID-19.

METHODS

Anti-SARS-CoV-2 Activity Assay. Vero cells were premixed with 20 μM of compounds for 4 h and then inoculated with MOI 0.05 of SARS-CoV-2 (0.05 mL/well). At least three wells were used as a negative control and were mock-infected, and three wells served as a virus control and were infected. All control wells were untreated. After 1 h of incubation at 37 $^{\circ}\text{C}$ at 5% CO_2 , wells were washed 3 times with dilution media, and 0.5 mL of media containing the indicated compound doses was added back to each well. 0.5 mL of dilution media per well was added to untreated wells. Cells were incubated at 37 $^{\circ}\text{C}$ at 5% CO_2 and samples collected at 0 and 24 h postinfection. Collected 100 μL time point media was replaced with an equal amount of compound doses or dilution media (untreated wells). Samples were stored at -80°C until the day of analysis. The SARS-CoV-2 titer in Vero cells via TCID₅₀ was performed for each sample collected at 0 and 24 h postinfection. These assays were performed in either duplicate or triplicate.

In Vitro Cytotoxicity Assay. Vero cells were cultured according to the manufacturer's protocol. The cells were adhered to wells in opaque 96-well plates by incubating 2×10^4 cells per well in 100 μL of Dulbecco's modified Eagle medium (DMEM) containing 7% fetal bovine serum (FBS) at 37 $^{\circ}\text{C}$ in a 5% CO_2 humidifying chamber for 24 hours. After discarding the media, the cells were then treated with either 11 or nicosamide in the range 0.024–25 μM in DMEM. After 72 h of incubation, an ATP-based assay was performed at 37 $^{\circ}\text{C}$ in a 5% CO_2 humidifying chamber for 10 min using the Cell Titer Glo luminescent cell viability assay kit (Promega, Madison, WI) per the manufacturer's instructions. The data was normalized to a positive control (DMEM with cells only and no drug), and the background using a negative control (0.2 mM digitonin in DMEM with cells) was subtracted. These assays were performed in duplicate.

Prophylactic Mouse Model of SARS-CoV-2. B6Cg-Tg(K18-ACE2)2Prlnm/J female mice (7–9 weeks of age) were used. Mice were maintained in pathogen-free conditions, and handling conforms to the requirements of the National Institutes of Health and the Scripps Research Institute Animal Research Committee. SARS-CoV-2 strain USA-WA1/2020 (BEI Resourced NR-52281) was grown on Vero cells using complete DMEM containing 10% FBS and 1 \times PenStrep. Mice were treated orally twice a day with either vehicle, EIDD-2801 (500 mg/kg), or compound 11 (5 mg/kg) starting 24 h preinfection. Mice were infected intranasally with 10^4 PFU/50 μL PBS. Weight loss was measured daily. Three independent trials were run with $n = 4$ mice treated with 11 to ensure consistency.

Quantification of Viral Titers and Cytokine Levels.

Lungs were collected in 1 mL of complete DMEM and proceeded with minibead beater bead homogenizer. Super-

natants were titrated on Vero cells; an overlay of 1% methyl cellulose was added, and plates were incubated at 37 °C for 3 days. Cells were fixed with PFA/PBS 4% and stained with crystal violet. Multiplex ELISA (Biorad; Hercules, CA) was performed to detect cytokines in BALF according to the manufacturer's instructions.

Statistics. Data is expressed as mean \pm SEM. An unpaired, one-tailed Student's *t*-test was calculated using GraphPad Prism to perform a statistical comparison between groups. A statistical comparison of two groups was performed by two-way ANOVA. Nonlinear regression curve-fitting of cell viability and viral activity was calculated using the log(inhibitor) vs response (variable slope) method in GraphPad Prism. One of several representative experiments was shown in each figure. Statistical limits and methods were determined according to our previous experience and published results obtained from SARS-CoV-2 infection as well as other viruses.^{35,36}

Chemistry: General Information. ¹H and ¹³C NMR spectra were recorded on a Bruker DRX-500 or a Bruker AV-400 instrument. The purity of the salicylanilides was determined to be 95% or greater by measuring the absorbance at 365 nm with HPLC. HPLC spectra were recorded on an Agilent Systems 1260 instrument using a Poroshell 120 EC-C8 column. The mobile phase gradient went from 50% H₂O in acetonitrile to 100% acetonitrile over 7 min and then isocratic at 100% acetonitrile for 3 min at a 0.5 mL/min flow rate.

General Procedure A: Synthesis of a 4-Chloro-(4-nitrophenoxy)benzene. A 4-chlorophenol (334 mg, 2.6 mmol) and a 4-halonitrobenzene (2.1 mmol) were dissolved in 2.4 mL of DMSO. Cesium carbonate (847.13 mg, 2.6 mmol) was added to the mixture. The resulting suspension was stirred either at room temperature or at 80 °C for 4 h when TLC monitoring indicated the completion of the reaction. The solution was diluted with 50 mL of DCM, washed with H₂O (4 \times 75 mL) to remove DMSO and salts, and washed with 75 mL of brine. The organic layer was dried with MgSO₄ and was then filtered and concentrated *in vacuo* to dryness. The concentrate was carried to the next step without further characterization.

General Procedure B: Synthesis of a 4-Chloro-(4-aminophenoxy)benzene. A 4-chloro-(4-nitrophenoxy)benzene (1.2 mmol) was dissolved in 3 mL of THF, 3 mL of ethanol (EtOH), and 1 mL of H₂O. To this solution were added elemental iron (670 mg, 12 mmol) and NH₄Cl (193 mg, 3.6 mmol). The mixture was refluxed for 2 h when TLC indicated completion of the reaction. The mixture was cooled to room temperature, diluted with 20 mL of ethyl acetate (EtOAc), and passed through a pad of Celite which was washed with EtOAc. The organic solution was washed with 40 mL of saturated NaHCO₃, 40 mL of H₂O, and 40 mL of brine. The organic layer was dried with MgSO₄ which was then filtered, and the filtrate was concentrated *in vacuo* to dryness. The concentrate was carried to the next step without further characterization.

General Procedure C: Synthesis of a Salicylanilide. A 4-chloro-(4-aminophenoxy)benzene (1.2 mmol) was dissolved in 5 mL of toluene. To this solution, 3,5-dichlorosalicylic acid (323 mg, 1.56 mmol) and then triphenylphosphite (403 μ L, 1.56 mmol) were added. The resulting suspension was refluxed for 12 h. The solution was concentrated *in vacuo* to dryness. The crude mixture was subjected to silica chromatography using a gradient of 0–10% DCM in methanol. Because some analogues coelute with an impurity, further purification must

be performed by first dissolving the concentrated, eluted crude mixture in a minimal amount of DCM and then precipitating the desired product with excess hexanes. After filtration, a white powder is obtained.

3,5-Dichloro-N-(4-(4-chlorophenoxy)phenyl)-2-hydroxybenzamide (1). Procedures A, then B, and finally C were performed. 54% yield over three steps. ¹H NMR (500 MHz, acetone-*d*₆): δ 7.05 (d, *J* = 9.0 Hz, 2H), 7.10 (d, *J* = 9.0 Hz, 2H), 7.41 (d, *J* = 9.0 Hz, 2H), 7.67 (d, *J* = 2.4 Hz, 1H), 7.79 (d, *J* = 9.0 Hz, 2H), 8.04 (d, *J* = 2.3 Hz, 1H), 10.01 (s, 1H), 13.06 (s, 1H). ¹³C NMR (125 MHz, acetone-*d*₆): δ 117.8, 120.2, 120.9, 123.5, 124.2, 124.5, 126.4, 128.7, 130.7, 134.1, 134.5, 154.9, 157.3, 157.5, 168.2. HRMS-ESI (*m/z*): [M + H]⁺ calcd for C₁₉H₁₂Cl₃NO₃, 407.9955; found, 407.9800. Purity by HPLC was found to be 100%.

N-(2-Bromo-4-(4-chlorophenoxy)phenyl)-3,5-dichloro-2-hydroxybenzamide (2). Procedures A, then B, and finally C were performed. 75% yield over three steps. ¹H NMR (500 MHz, acetone-*d*₆): δ 7.14 (d, *J* = 8.7 Hz, 3H), 7.37 (d, *J* = 2.5 Hz, 1H), 7.46 (d, *J* = 8.8 Hz, 2H), 7.71 (s, 1H), 7.82 (d, *J* = 8.8 Hz, 1H), 8.08 (s, 1H), 9.96 (s, 1H), 12.61 (s, 1H). ¹³C NMR (125 MHz, acetone-*d*₆): δ 118.1, 119.0, 121.2, 121.9, 123.3, 124.1, 124.3, 127.1, 129.7, 130.0, 131.0, 131.6, 134.6, 156.2, 156.7, 157.1, 168.0. HRMS-ESI (*m/z*): [M + H]⁺ calcd for C₁₉H₁₁BrCl₃NO₃, 485.9061; found, 485.8909. Purity by HPLC was found to be 100%.

N-(3-Bromo-4-(4-chlorophenoxy)phenyl)-3,5-dichloro-2-hydroxybenzamide (3). Procedures A, then B, and finally C were performed. 62% yield over three steps. ¹H NMR (500 MHz, acetone-*d*₆): δ 7.00 (dt, *J* = 2.3, 9.0 Hz, 2H), 7.19 (d, *J* = 8.8 Hz, 1H), 7.41 (dt, *J* = 2.3, 9.0 Hz, 2H), 7.70 (d, *J* = 2.4 Hz, 1H), 7.80 (dd, *J* = 2.6, 8.9 Hz, 1H), 8.04 (d, *J* = 2.4 Hz, 1H), 8.22 (d, *J* = 2.6 Hz, 1H), 10.07 (s, 1H), 12.79 (s, 1H). ¹³C NMR (125 MHz, acetone-*d*₆): δ 115.4, 117.8, 119.9, 122.4, 123.4, 123.7, 124.3, 126.6, 127.6, 128.7, 130.7, 134.7, 135.8, 150.8, 157.0, 157.4, 168.3. HRMS-ESI (*m/z*): [M + H]⁺ calcd for C₁₉H₁₁BrCl₃NO₃, 485.9061; found, 485.8906. Purity by HPLC was found to be 100%.

3,5-Dichloro-N-(3-chloro-4-(4-chlorophenoxy)phenyl)-2-hydroxybenzamide (4). Procedures A, then B, and finally C were performed. 39% yield over three steps. ¹H NMR (500 MHz, acetone-*d*₆): δ 7.00 (dt, *J* = 2.2, 9 Hz, 2H), 7.21 (d, *J* = 8.9 Hz, 1H), 7.41 (dt, *J* = 2.2, 9 Hz, 2H), 7.70 (d, *J* = 2.4 Hz, 1H), 7.75 (dd, *J* = 2.6, 8.9 Hz, 1H), 8.04 (d, *J* = 2.5 Hz, 1H), 8.07 (d, *J* = 2.6 Hz, 1H), 10.09 (s, 1H), 12.78 (s, 1H). ¹³C NMR (125 MHz, acetone-*d*₆): δ 117.8, 119.7, 122.7, 123.7, 124.3, 124.6, 126.6, 128.7, 130.7, 134.7, 135.7, 149.6, 157.1, 157.4, 168.3. HRMS-ESI (*m/z*): [M + H]⁺ calcd for C₁₉H₁₁Cl₄NO₃, 441.9566; found, 441.9407. Purity by HPLC was found to be 100%.

3,5-Dichloro-N-(4-(4-chlorophenoxy)-3-iodophenyl)-2-hydroxybenzamide (5). Procedures A, then B, and finally C were performed. 52% yield over three steps. ¹H NMR (500 MHz, acetone-*d*₆): δ 6.99 (d, *J* = 8.95 Hz, 2H), 7.09 (d, *J* = 8.8 Hz, 1H), 7.41 (d, *J* = 9.0 Hz, 2H), 7.84 (dd, *J* = 2.5, 8.8 Hz, 1H), 8.04 (d, *J* = 2.4 Hz, 1H), 8.38 (d, *J* = 2.5 Hz, 1H), 10.01 (s, 1H), 12.83 (s, 1H). ¹³C NMR (125 MHz, acetone-*d*₆): δ 89.3, 117.8, 120.0, 121.1, 123.6, 124.2, 124.3, 126.6, 128.7, 130.8, 133.6, 134.7, 135.8, 153.9, 157.1, 157.4, 168.3. HRMS-ESI (*m/z*): [M + H]⁺ calcd for C₁₉H₁₁Cl₃INO₃, 533.8922; found, 533.8758. Purity by HPLC was found to be 100%.

3,5-Dichloro-N-(4-(4-chlorophenoxy)-3-fluorophenyl)-2-hydroxybenzamide (6). Procedures A, then B, and finally C

were performed. 69% yield over three steps. ^1H NMR (500 MHz, acetone- d_6): δ 7.03 (d, J = 8.9 Hz, 2H), 7.25 (t, J = 8.9 Hz, 1H), 7.40 (d, J = 9.0 Hz, 2H), 7.58 (d, J = 8.8 Hz, 1H), 7.69 (d, J = 2.4 Hz, 1H), 7.88 (dd, J = 2.3, 12.8 Hz, 1H), 8.02 (d, 2.25 Hz, 1H), 10.11 (s, 1H), 12.77 (s, 1H). ^{13}C NMR (125 MHz, acetone- d_6): δ 111.5, 111.7, 119.0, 119.1, 119.2, 123.4, 123.7, 124.3, 126.5, 128.5, 130.7, 134.7, 135.8, 135.9, 153.7, 155.7, 157.3, 157.5, 168.3. HRMS-ESI (m/z): $[\text{M} + \text{H}]^+$ calcd for $\text{C}_{19}\text{H}_{11}\text{Cl}_3\text{FNO}_3$, 425.9861; found, 425.9701. Purity by HPLC was found to be 100%.

3,5-Dichloro-*N*-(4-(4-chlorophenoxy)-3-methoxyphenyl)-2-hydroxybenzamide (7). Procedures A, then B, and finally C were performed. 57% yield over three steps. ^1H NMR (500 MHz, acetone- d_6): δ 3.80 (s, 3H), 6.89 (dt, J = 3.5, 9.1 Hz, 2H), 7.12 (d, 8.65 Hz, 1H), 7.32 (dt, J = 3.5, 9.1 Hz, 2H), 7.40 (dt, J = 2.8, 8.7 Hz, 1H), 7.66 (t, J = 2.6 Hz, 1H), 7.70 (d, J = 2.4 Hz, 1H), 8.04 (d, J = 2.3 Hz, 1H), 10.08 (s, 1H), 12.98 (s, 1H). ^{13}C NMR (125 MHz, acetone- d_6): δ 56.3, 108.2, 115.1, 117.9, 118.4, 123.0, 123.6, 124.2, 126.5, 127.2, 130.3, 134.5, 136.1, 141.8, 152.8, 157.4, 158.4, 168.2. HRMS-ESI (m/z): $[\text{M} + \text{H}]^+$ calcd for $\text{C}_{20}\text{H}_{14}\text{Cl}_3\text{NO}_4$, 438.0061; found, 437.9902. Purity by HPLC was found to be 100%.

3,5-Dichloro-*N*-(4-(4-chlorophenoxy)-2-methoxyphenyl)-2-hydroxybenzamide (8). Procedures A, then B, and finally C were performed. 59% yield over three steps. ^1H NMR (500 MHz, acetone- d_6): δ 3.90 (s, 3H), 6.65 (dd, J = 2.4, 8.7 Hz, 1H), 6.87 (d, J = 2.3 Hz, 1H), 7.07 (d, J = 8.9 Hz, 2H), 7.41 (d, J = 9.0 Hz, 2H), 7.69 (d, J = 2.4 Hz, 1H), 7.99 (t, J = 8.4 Hz, 1H), 8.05 (s, 1H), 9.69 (s, 1H), 12.65 (s, 1H). ^{13}C NMR (125 MHz, acetone- d_6): δ 56.6, 104.1, 111.1, 118.8, 120.9, 122.8, 124.0, 124.2, 125.7, 127.1, 128.7, 130.7, 134.3, 153.7, 155.9, 156.4, 157.2, 167.1. HRMS-ESI (m/z): $[\text{M} + \text{H}]^+$ calcd for $\text{C}_{20}\text{H}_{14}\text{Cl}_3\text{NO}_4$, 438.0061; found, 437.9902. Purity by HPLC was found to be 95%.

3,5-Dichloro-*N*-(4-(4-chlorophenoxy)-3-cyanophenyl)-2-hydroxybenzamide (9). Procedures A, then B, and finally C were performed. 52% yield over three steps. ^1H NMR (500 MHz, acetone- d_6): δ 7.14 (d, J = 9.1 Hz, 1H), 7.22 (d, J = 8.9 Hz, 2H), 7.50 (d, J = 9.0 Hz, 2H), 7.70, (d, J = 2.4 Hz, 1H), 8.01 (d, J = 8.0 Hz, 1H), 8.03 (d, J = 2.3 Hz, 1H), 8.25 (s, 1H), 10.20 (s, 1H), 12.71 (s, 1H). ^{13}C NMR (125 MHz, acetone- d_6): δ 105.1, 115.9, 117.7, 119.6, 121.9, 123.8, 124.3, 126.6, 127.4, 129.1, 130.4, 131.1, 134.2, 134.8, 155.5, 156.6, 157.3, 168.5. HRMS-ESI (m/z): $[\text{M} + \text{H}]^+$ calcd for $\text{C}_{20}\text{H}_{11}\text{Cl}_3\text{N}_2\text{O}_3$, 432.9908; found, 432.9754. Purity by HPLC was found to be 100%.

3,5-Dichloro-*N*-(4-(4-chlorophenoxy)-2-iodophenyl)-2-hydroxybenzamide (10). Procedures A, then B, and finally C were performed. 72% yield over three steps. ^1H NMR (500 MHz, acetone- d_6): δ 7.11–7.14 (m, 2H), 7.15 (dd, J = 2.8, 13.2 Hz, 1H), 7.43–7.47 (m, 2H), 7.59 (d, J = 2.8 Hz, 1H), 7.66 (d, J = 8.8 Hz, 1), 7.70 (d, J = 2.5 Hz, 1H), 8.10 (d, J = 2.5 Hz, 1H), 9.90 (s, 1H), 12.82 (s, 1H). ^{13}C NMR (125 MHz, acetone- d_6): δ 98.0, 117.7, 119.8, 121.9, 123.9, 124.3, 126.8, 129.5, 129.7, 130.0, 130.1, 134.7, 156.2, 157.2, 168.5. HRMS-ESI (m/z): $[\text{M} + \text{H}]^+$ calcd for $\text{C}_{19}\text{H}_{11}\text{Cl}_3\text{INO}_3$, 533.8922; found, 533.8761. Purity by HPLC was found to be 96%.

3,5-Dichloro-*N*-(4-(4-chlorophenoxy)-3,5-bis(trifluoromethyl)phenyl)-2-hydroxybenzamide (11). Procedures A using 17 as the 4-halonitrobenzene, then B, and finally C were performed. 57% yield over three steps. ^1H NMR (500 MHz, acetone- d_6): δ 6.88–6.93 (m, 2H), 7.35–7.39 (m, 2H),

7.73 (d, J = 2.5 Hz, 1H), 8.10 (d, J = 2.5 Hz, 1H), 8.59 (s, 2H), 10.65 (s, 1H). ^{13}C NMR (125 MHz, acetone- d_6): δ 117.8, 122.3, 123.9, 124.4, 124.5, 125.2, 126.8, 126.9, 127.2, 128.3, 130.3, 135.11, 137.0, 157.3, 159.2, 168.7. HRMS-ESI (m/z): $[\text{M} + \text{H}]^+$ calcd for $\text{C}_{21}\text{H}_{10}\text{Cl}_3\text{F}_6\text{NO}_3$, 543.9703; found, 543.9543. Purity by HPLC was found to be 100%.

3,5-Dichloro-*N*-(4-(4-chlorophenoxy)-3,5-diiodophenyl)-2-hydroxybenzamide (12). Procedures A using 18 as the 4-halonitrobenzene, then B, and finally C were performed. 51% yield over three steps. ^1H NMR (500 MHz, DMSO- d_6): δ 6.80 (d, J = 8.5 Hz, 2H), 7.40 (d, J = 8.8 Hz, 2H), 7.82, (s, 1H), 8.02 (s, 1H), 8.33 (s, 2H), 10.82 (s, 1H). ^{13}C NMR (125 MHz, acetone- d_6): δ 90.9, 117.7, 117.9, 123.8, 124.3, 126.7, 127.8, 130.6, 133.7, 134.9, 137.9, 151.6, 156.2, 156.9, 157.3, 168.4. HRMS-ESI (m/z): $[\text{M} + \text{H}]^+$ calcd for $\text{C}_{19}\text{H}_{10}\text{Cl}_3\text{I}_2\text{NO}_3$, 659.7889; found, 659.7720. Purity by HPLC was found to be 100%.

3,5-Dichloro-*N*-(4-(4-chlorophenoxy)-3,5-dinitrophenyl)-2-hydroxybenzamide (13). 3,5-Dichlorosalicylic acid (200 mg, 0.97 mmol) was dissolved in 6.8 mL of dry methylene chloride under argon. After adding thionyl chloride (140 μL , 1.94 mmol), the resulting solution was stirred at 40 $^\circ\text{C}$ overnight. The mixture was concentrated *in vacuo* to dryness to yield the acid chloride. The aniline product (309 mg, 1 mmol) of Procedure A that used 20 as the 4-halonitrobenzene was dissolved in 2 mL of ethanol along with diisopropylethylamine (540 μL , 3 mmol) and cooled to 0 $^\circ\text{C}$. This cooled solution was added to the acid chloride. The resulting solution was refluxed overnight. Upon cooling the solution to room temperature, it was concentrated *in vacuo* and subjected to silica chromatography using hexanes and ethyl acetate (1:1) as the mobile phase to yield an off-white powder (7 mg, 1.4% yield). ^1H NMR (400 MHz, acetone- d_6): δ 7.03–7.08 (m, 2H), 7.36–7.41 (m, 2H), 7.70 (d, J = 2.5 Hz, 1H), 8.08 (d, J = 2.5 Hz, 1H), 8.88 (s, 2H). ^{13}C NMR (125 MHz, acetone- d_6): δ 117.9, 118.0, 122.8, 123.4, 124.7, 127.1, 129.0, 130.6, 135.1, 136.9, 137.7, 145.4, 157.4, 157.7, 168.7. HRMS-ESI (m/z): $[\text{M} + \text{H}]^+$ calcd for $\text{C}_{19}\text{H}_{10}\text{Cl}_3\text{N}_3\text{O}_7$, 497.9657; found, 497.9496. Purity by HPLC was found to be 100%.

***N,N'*-(((Perfluoropropane-2,2-diyl)bis(4,1-phenylene))bis(oxy))bis(4,1-phenylene)bis(3,5-dichloro-2-hydroxybenzamide) (14)**. Procedure C was followed using 4,4'-(((perfluoropropane-2,2-diyl)bis(4,1-phenylene))bis(oxy))dianiline (321.4 mg, 0.62 mmol) as the aniline. The yield was 72%. ^1H NMR (400 MHz, CDCl_3): δ 6.98 (dt, J = 2.1, 9.05 Hz, 4H), 7.12 (dt, J = 3.3, 8.90 Hz, 4H), 7.36 (d, J = 8.70 Hz, 4H), 7.51 (d, J = 2.35 Hz, 2H), 7.56 (d, J = 2.40 Hz, 2H), 7.58 (dt, J = 2.15, 8.95 Hz, 4H), 8.73 (s, 2H), 12.10 (bs, 2H). ^{13}C NMR (125 MHz, acetone- d_6): δ 117.9, 118.5, 121.1, 123.7, 124.3, 124.6, 126.6, 128.2, 132.8, 134.6, 134.7, 154.0, 157.6, 159.5, 168.4. ESI-TOF (m/z): $[\text{M} + \text{H}]^+$ calcd for $\text{C}_{41}\text{H}_{24}\text{Cl}_4\text{F}_6\text{N}_2\text{O}_6$, 893.9; found, 894.0. Purity by HPLC was found to be 98%.

3,5-Dichloro-*N*-(4-(4-chloro-3,5-dimethoxyphenoxy)-3,5-bis(trifluoromethyl)phenyl)-2-hydroxybenzamide (15). Procedures A, then B, and finally C were performed. 74% yield over three steps. ^1H NMR (500 MHz, DMSO- d_6): δ 3.32 (s, 6H), 6.07 (s, 2H), 6.98 (dt, J = 3.30, 8.95 Hz, 2H), 7.25 (s, 2H), 7.43 (dt, J = 3.35, 8.95 Hz, 2H). ^{13}C NMR (125 MHz, acetone- d_6): δ 57.4, 94.6, 105.9, 118.3, 124.5, 125.0, 125.6, 125.7, 127.3, 127.5, 127.8, 135.7, 137.6, 157.7, 158.2, 169.2. ESI-TOF (m/z): $[\text{M} + \text{H}]^+$ calcd for $\text{C}_{23}\text{H}_{14}\text{Cl}_3\text{F}_6\text{NO}_5$, 602.98; found, 602.9. Purity by HPLC was found to be 98%.

N-(4-Chlorophenyl)-2-hydroxy-3,5-diiodobenzamide (**16**). The synthesis of the title compound followed literature procedures.²⁴ Purity by HPLC was found to be 100%.

2-Bromo-5-nitro-1,3-bis(trifluoromethyl)benzene (17). 2-Bromo-1,3-bis(trifluoromethyl)benzene (2 g, 6.82 mmol) was added to a mixture of 4.2 mL of concentrated H₂SO₄ and 3 mL of fuming HNO₃. The solution was heated at 70 °C for 2 h, cooled to room temperature, and poured onto 200 mL of ice water. The precipitate was filtered and dissolved in 100 mL of ethyl acetate and washed with 100 mL of H₂O to remove residual acid. The organic layer was dried with MgSO₄ which was then removed with filtration, and the filtrate was concentrated *in vacuo* to dryness to afford an off-white powder (2.19 g, 95% yield). ¹H NMR (400 MHz, CDCl₃): δ 8.73 (s, 2H).

2-Fluoro-1,3-diiodo-5-nitrobenzene (18). 4-Nitro-1-fluorobenzene (113 μL, 1.06 mmol) was mixed in triflic acid (1 mL, 10.6 mmol) and cooled to 0 °C. *N*-Iodosuccinimide (525 mg, 2.33 mmol) was added in portions to the cooled solution. The solution was warmed to room temperature and stirred for 4 h, at which point an additional portion of *N*-iodosuccinimide (137 mg, 0.61 mmol) was added and stirred overnight. Since TLC monitoring did not show the completion of reaction, an additional portion of *N*-iodosuccinimide (200 mg, 0.89 mmol) and triflic acid (1 mL, 10.6 mmol) were added and stirred over a second night. The reaction mixture was quenched with cold H₂O, extracted with methylene chloride, and washed with 10% sodium bisulfite, H₂O, and then brine. The organic layer was dried with MgSO₄ which was then removed with filtration, and the filtrate was concentrated *in vacuo* to dryness to afford a yellow powder (393 mg, 94% yield) which was carried to the next step without further characterization.

4-Fluoro-3,5-dinitrobenzoic acid (19). A mixture of H₂SO₄ (22.5 mL) containing 30% SO₃ and fuming HNO₃ was cooled to 0 °C. To the cooled solution, 4-fluorobenzoic acid (5 g, 35.8 mmol) was added slowly to not exceed 20 °C. The solution was heated at 85 °C for 10 min, cooled to 40 °C, and then heated at 95 °C for an additional 3 h. After cooling the mixture to room temperature, it was poured over ice water, and the resulting precipitate was collected by filtration to yield a yellow powder (5.6 g, 68% yield). ¹H NMR (400 MHz, acetone-*d*₆): δ 8.96 (d, *J* = 6.3 Hz, 2H).

4-Fluoro-3,5-dinitroaniline (20). After cooling H₂SO₄ (15 mL) containing 20% SO₃ to 0 °C, **19** (5.5 g, 24.3 mmol) was added, followed by ethylene chloride (20 mL). Sodium azide (1.81 g, 27.9 mmol) was added in portions to the cooled solution to not exceed 20 °C. The solution was then heated at reflux for 1 h, cooled to room temperature, and poured over ice water, and the resulting precipitate was collected by filtration to yield an orange powder (4.0 g, 82% yield). ¹H NMR (500 MHz, MeOD): δ 7.51 (d, *J* = 5.4 Hz, 2H). ESI-TOF (*m/z*): [M + H]⁺ calcd for C₆H₄FN₃O₄, 202.02; found, 202.1.

■ ASSOCIATED CONTENT

SI Supporting Information

The Supporting Information is available free of charge at <https://pubs.acs.org/doi/10.1021/acsinfecdis.1c00253>.

Relative weight change of mice treated with vehicle and **11** and percent neutralization of viral activity in **7**, **12**, and **14–16** (PDF)

■ AUTHOR INFORMATION

Corresponding Author

Kim D. Janda – Departments of Chemistry and Immunology, The Skaggs Institute for Chemical Biology, Worm Institute of Research and Medicine (WIRM), The Scripps Research Institute, La Jolla, California 92037, United States; orcid.org/0000-0001-6759-4227; Phone: (858) 785-2515; Email: kdjanda@scripps.edu; Fax: (858) 784-2595

Authors

Steven Blake – Departments of Chemistry and Immunology, The Skaggs Institute for Chemical Biology, Worm Institute of Research and Medicine (WIRM), The Scripps Research Institute, La Jolla, California 92037, United States; orcid.org/0000-0002-3357-0515

Namir Shaabani – Department of Immunology and Microbiology, The Scripps Research Institute, La Jolla, California 92037, United States

Lisa M. Eubanks – Departments of Chemistry and Immunology, The Skaggs Institute for Chemical Biology, Worm Institute of Research and Medicine (WIRM), The Scripps Research Institute, La Jolla, California 92037, United States; orcid.org/0000-0001-5288-6294

Junki Maruyama – Department of Pathology, University of Texas Medical Branch, Galveston, Texas 77555, United States

John T. Manning – Department of Pathology, University of Texas Medical Branch, Galveston, Texas 77555, United States

Nathan Beutler – Department of Immunology and Microbiology, The Scripps Research Institute, La Jolla, California 92037, United States

Slobodan Paessler – Department of Pathology, University of Texas Medical Branch, Galveston, Texas 77555, United States

Henry Ji – Sorrento Therapeutics Inc., San Diego, California 92121, United States

John R. Teijaro – Department of Immunology and Microbiology, The Scripps Research Institute, La Jolla, California 92037, United States

Complete contact information is available at: <https://pubs.acs.org/doi/10.1021/acsinfecdis.1c00253>

Author Contributions

¹S.B. and N.S. contributed equally. All authors have given approval to the final version of the manuscript.

Funding

S.P. has received funding from Sorrento Therapeutics for their part of the work presented in this paper. The other authors have no funding to declare.

Notes

The authors declare the following competing financial interest(s): S.P. holds stock options of Sorrento Therapeutics company.

■ ACKNOWLEDGMENTS

We thank Amanda Roberts from the Mouse Behavioral Assessment Core Facility at Scripps Research for technical support on animal experiments. This project was supported by the Skaggs Institute for Chemical Biology.

REFERENCES

- (1) Cutler, D. M., and Summers, L. H. (2020) The COVID-19 Pandemic and the \$16 Trillion Virus. *J. Am. Med. Assoc.* 324, 1495–1496.
- (2) Parasher, A. (2021) COVID-19: Current understanding of its Pathophysiology, Clinical presentation and Treatment. *Postgrad. Med. J.* 97, 312–320.
- (3) Wan, Y., Shang, J., Graham, R., Baric, R. S., and Li, F. (2020) Receptor recognition by the novel coronavirus from Wuhan: an analysis based on decade-long structural studies of SARS coronavirus. *J. Virol.* 94, 1–9.
- (4) Bayati, A., Kumar, R., Francis, V., and McPherson, P. S. (2021) SARS-CoV-2 infects cells after viral entry via clathrin-mediated endocytosis. *J. Biol. Chem.* 296, 1–12.
- (5) Staring, J., Raaben, M., and Brummelkamp, T. R. (2018) Viral escape from endosomes and host detection at a glance. *J. Cell Sci.* 131, 1–8.
- (6) Aschwanden, C. (2021) Five reasons why COVID herd immunity is probably impossible. *Nature* 591, 520–522.
- (7) Beigel, J. H., Tomashek, K. M., Dodd, L. E., Mehta, A. K., Zingman, B. S., Kalil, A. C., Hohmann, E., Chu, H. Y., Luetkemeyer, A., and Kline, S. (2020) Remdesivir for the treatment of Covid-19—preliminary report. *N. Engl. J. Med.* 383, 992–994.
- (8) Kalil, A. C., Patterson, T. F., Mehta, A. K., Tomashek, K. M., Wolfe, C. R., Ghazaryan, V., Marconi, V. C., Ruiz-Palacios, G. M., Hsieh, L., and Kline, S. (2021) Baricitinib plus remdesivir for hospitalized adults with Covid-19. *N. Engl. J. Med.* 384, 795–807.
- (9) Chen, P., Nirula, A., Heller, B., Gottlieb, R. L., Boscia, J., Morris, J., Huhn, G., Cardona, J., Mocherla, B., and Stosor, V. (2021) SARS-CoV-2 neutralizing antibody LY-CoV555 in outpatients with Covid-19. *N. Engl. J. Med.* 384, 229–237.
- (10) Hoffmann, M., Arora, P., Groß, R., Seidel, A., Hörnich, B. F., Hahn, A. S., Krüger, N., Graichen, L., Hofmann-Winkler, H., and Kempf, A. (2021) SARS-CoV-2 variants B.1.351 and P.1 escape from neutralizing antibodies. *Cell* 184, 2384–2393.
- (11) Wang, P., Nair, M. S., Liu, L., Iketani, S., Luo, Y., Guo, Y., Wang, M., Yu, J., Zhang, B., Kwong, P. D., Graham, B. S., Mascola, J. R., Chang, J. Y., Yin, M. T., Sobieszczyk, M., Kyrytsous, C. A., Shapiro, L., Sheng, Z., Huang, Y., and Ho, D. D. (2021) Antibody resistance of SARS-CoV-2 variants B.1.351 and B.1.1.7. *Nature* 593, 130–135.
- (12) Jurgeit, A., McDowell, R., Moese, S., Meldrum, E., Schwendener, R., and Greber, U. F. (2012) Niclosamide Is a Proton Carrier and Targets Acidic Endosomes with Broad Antiviral Effects. *PLoS Pathog.* 8, No. e1002976.
- (13) Stachulski, A. V., Pidathala, C., Row, E. C., Sharma, R., Berry, N. G., Lawrenson, A. S., Moores, S. L., Iqbal, M., Bentley, J., and Allman, S. A. (2011) Thiazolidines as novel antiviral agents. 2. Inhibition of hepatitis C virus replication. *J. Med. Chem.* 54, 8670–8680.
- (14) Wen, C.-C., Kuo, Y.-H., Jan, J.-T., Liang, P.-H., Wang, S.-Y., Liu, H.-G., Lee, C.-K., Chang, S.-T., Kuo, C.-J., and Lee, S.-S. (2007) Specific plant terpenoids and lignoids possess potent antiviral activities against severe acute respiratory syndrome coronavirus. *J. Med. Chem.* 50, 4087–4095.
- (15) Zhang, X. W., and Yap, Y. L. (2004) Old drugs as lead compounds for a new disease? Binding analysis of SARS coronavirus main proteinase with HIV, psychotropic and parasite drugs. *Bioorg. Med. Chem.* 12, 2517–2521.
- (16) Xu, J., Shi, P.-Y., Li, H., and Zhou, J. (2020) Broad Spectrum Antiviral Agent Niclosamide and Its Therapeutic Potential. *ACS Infect. Dis.* 6, 909–915.
- (17) Li, Z., Brecher, M., Deng, Y.-Q., Zhang, J., Sakamuru, S., Liu, B., Huang, R., Koetzner, C. A., Allen, C. A., Jones, S. A., Chen, H., Zhang, N.-N., Tian, M., Gao, F., Lin, Q., Banavali, N., Zhou, J., Boles, N., Xia, M., Kramer, L. D., Qin, C.-F., and Li, H. (2017) Existing drugs as broad-spectrum and potent inhibitors for Zika virus by targeting NS2B-NS3 interaction. *Cell Res.* 27, 1046–1064.
- (18) Gassen, N. C., Niemyer, D., Muth, D., Corman, V. M., Martinelli, S., Gassen, A., Hafner, K., Papias, J., Mösbauer, K., Zellner, A., Zannas, A. S., Herrmann, A., Holsboer, F., Brack-Werner, R., Boshart, M., Müller-Myhsok, B., Drosten, C., Müller, M. A., and Rein, T. (2019) SKP2 attenuates autophagy through Beclin1-ubiquitination and its inhibition reduces MERS-Coronavirus infection. *Nat. Commun.* 10, 5770.
- (19) Kadri, H., Lambourne, O. A., and Mehellou, Y. (2018) Niclosamide, a drug with many (re) purposes. *ChemMedChem* 13, 1088–1091.
- (20) Lin, C.-K., Bai, M.-Y., Hu, T.-M., Wang, Y.-C., Chao, T.-K., Weng, S.-J., Huang, R.-L., Su, P.-H., and Lai, H.-C. (2016) Preclinical evaluation of a nanoformulated anthelmintic, niclosamide, in ovarian cancer. *Oncotarget* 7, 8993–9006.
- (21) Martin, R. J. (1997) Modes of action of anthelmintic drugs. *Vet. J.* 154, 11–34.
- (22) Gooyit, M., Tricoche, N., Lustigman, S., and Janda, K. D. (2014) Dual protonophore–Chitinase inhibitors dramatically affect *O. volvulus* molting. *J. Med. Chem.* 57, 5792–5799.
- (23) Blake, S., Thanissery, R., Rivera, A. J., Hixon, M. S., Lin, M., Theriot, C. M., and Janda, K. D. (2020) Salicylanilide Analog Minimizes Relapse of *Clostridioides difficile* Infection in Mice. *J. Med. Chem.* 63, 6898–6908.
- (24) Gooyit, M., and Janda, K. D. (2016) Reprofiled anthelmintics abate hypervirulent stationary-phase *Clostridium difficile*. *Sci. Rep.* 6, 1–8.
- (25) Study of Niclosamide in Moderate and Severe Hospitalized Coronavirus-19 (COVID-19) Patients. <https://ClinicalTrials.gov/show/NCT04603924>.
- (26) Niclosamide for Mild to Moderate COVID-19. <https://ClinicalTrials.gov/show/NCT04399356>.
- (27) Rosenke, K., Hansen, F., Schwarz, B., Feldmann, F., Haddock, E., Rosenke, R., Barbian, K., Meade-White, K., Okumura, A., Leventhal, S., Hawman, D. W., Ricotta, E., Bosio, C. M., Martens, C., Saturday, G., Feldmann, H., and Jarvis, M. A. (2021) Orally delivered MK-4482 inhibits SARS-CoV-2 replication in the Syrian hamster model. *Nat. Commun.* 12, 1–8.
- (28) Stuyver, L. J., Whitaker, T., McBrayer, T. R., Hernandez-Santiago, B. I., Lostia, S., Tharnish, P. M., Ramesh, M., Chu, C. K., Jordan, R., and Shi, J. (2003) Ribonucleoside analogue that blocks replication of bovine viral diarrhoea and hepatitis C viruses in culture. *Antimicrob. Agents Chemother.* 47, 244–254.
- (29) Ye, Q., Wang, B., and Mao, J. (2020) The pathogenesis and treatment of the Cytokine Storm in COVID-19. *J. Infect.* 80, 607–613.
- (30) Herold, T., Jurinovic, V., Arnreich, C., Lipworth, B. J., Hellmuth, J. C., von Bergwelt-Baildon, M., Klein, M., and Weinberger, T. (2020) Elevated levels of IL-6 and CRP predict the need for mechanical ventilation in COVID-19. *J. Allergy Clin. Immunol.* 146, 128–136.
- (31) Jørgensen, M. J., Holter, J. C., Christensen, E. E., Schjalm, C., Tonby, K., Pischke, S. E., Jennum, S., Skeie, L. G., Nur, S., and Lind, A. (2020) Increased interleukin-6 and macrophage chemoattractant protein-1 are associated with respiratory failure in COVID-19. *Sci. Rep.* 10, 1–11.
- (32) Xi, X., Guo, Y., Zhu, M., Wei, Y., Li, G., Du, B., and Wang, Y. (2021) Higher expression of monocyte chemotactic protein 1 in mild COVID-19 patients might be correlated with inhibition of Type I IFN signaling. *Virol. J.* 18, 1–7.
- (33) Xu, Z.-S., Shu, T., Kang, L., Wu, D., Zhou, X., Liao, B.-W., Sun, X.-L., Zhou, X., and Wang, Y.-Y. (2020) Temporal profiling of plasma cytokines, chemokines and growth factors from mild, severe and fatal COVID-19 patients. *Signal Transduct. Target. Ther.* 5, 1–3.
- (34) Zhao, Y., Kilian, C., Turner, J.-E., Bosurgi, L., Roedl, K., Bartsch, P., Gnirck, A.-C., Cortesi, F., Schultheiß, C., Hellmig, M., Enk, L. U. B., Hausmann, F., Borchers, A., Wong, M. N., Paust, H.-J., Siracusa, F., Scheibel, N., Herrmann, M., Rosati, E., Bacher, P., Kyllies, D., Jarczak, D., Lütgehetmann, M., Pfefferle, S., Steurer, S., Schulze zur Wiesch, J., Puelles, V. G., Sperhake, J.-P., Addo, M. M., Lohse, A. W., Binder, M., Huber, S., Huber, T. B., Kluge, S., Bonn, S., Panzer, U., Gagliani, N., and Krebs, C. F. (2021) Clonal expansion and

activation of tissue-resident memory-like T_H17 cells expressing GM-CSF in the lungs of patients with severe COVID-19. *Sci. Immunol.* 6, No. eabf6692.

(35) Rogers, T. F., Zhao, F., Huang, D., Beutler, N., Burns, A., He, W.-t., Limbo, O., Smith, C., Song, G., Woehl, J., Yang, L., Abbott, R. K., Callaghan, S., Garcia, E., Hurtado, J., Parren, M., Peng, L., Ramirez, S., Ricketts, J., Ricciardi, M. J., Rawlings, S. A., Wu, N. C., Yuan, M., Smith, D. M., Nemazee, D., Teijaro, J. R., Voss, J. E., Wilson, I. A., Andrabi, R., Briney, B., Landais, E., Sok, D., Jardine, J. G., and Burton, D. R. (2020) Isolation of potent SARS-CoV-2 neutralizing antibodies and protection from disease in a small animal model. *Science* 369, 956–963.

(36) Shaabani, N., Duhan, V., Khairnar, V., Gassa, A., Ferrer-Tur, R., Häussinger, D., Recher, M., Zelinskyy, G., Liu, J., Dittmer, U., Trilling, M., Scheu, S., Hardt, C., Lang, P. A., Honke, N., and Lang, K. S. (2016) CD169+ macrophages regulate PD-L1 expression via type I interferon and thereby prevent severe immunopathology after LCMV infection. *Cell Death Dis.* 7, e2446–e2446.